Solar Phys (2007) 246: 365–391
DOI 10.1007/s11207-007-9061-z

Transient Coronal Sigmoids and Rotating Erupting Flux Ropes

L.M. Green · B. Kliem · T. Török · L. van Driel-Gesztelyi · G.D.R. Attrill

Received: 2 January 2007 / Accepted: 21 September 2007 / Published online: 13 November 2007

Abstract To determine the relationship between transient coronal (soft X-ray or EUV) sigmoids and erupting flux ropes, we analyse four events in which a transient sigmoid could be associated with a filament whose apex rotates upon eruption and two further events in which the two phenomena were spatially but not temporally coincident. We find the helicity sign of the erupting field and the direction of filament rotation to be consistent with the conversion of twist into writhe under the ideal MHD constraint of helicity conservation, thus supporting our assumption of flux rope topology for the rising filament. For positive (negative) helicity the filament apex rotates clockwise (counterclockwise), consistent with the flux rope taking on a reverse (forward) S shape, which is opposite to that observed for the sigmoid. This result is incompatible with two models for sigmoid formation: one identifying sigmoids with upward arching kink-unstable flux ropes and one identifying sigmoids with a current layer between two oppositely sheared arcades. We find instead that the observations agree well with the model by Titov and Démoulin (*Astron. Astrophys.* **351**, 707, 1999), which identifies transient sigmoids with steepened current layers below rising flux ropes.

Keywords Sun: sigmoids · Sun: flux rope · Sun: magnetic fields · Sun: eruptions

L.M. Green (✉) · T. Török · L. van Driel-Gesztelyi · G.D.R. Attrill
University College London, Mullard Space Science Laboratory, Holmbury St. Mary, Dorking, Surrey, RH5 6NT, UK
e-mail: lmg@mssl.ucl.ac.uk

B. Kliem
Astrophysikalisches Institut Potsdam, An der Sternwarte 16, 14482 Potsdam, Germany

B. Kliem
Kiepenheuer-Institut für Sonnenphysik, Schöneckstr. 6, 79104 Freiburg, Germany

L. van Driel-Gesztelyi
Observatoire de Paris, LESIA, FRE 2461 (CNRS), 92195 Meudon Principal Cedex, France

L. van Driel-Gesztelyi
Konkoly Observatory of the Hungarian Academy of Sciences, Budapest, Hungary

1. Introduction

The presence of S-shaped features on the Sun has been known for several decades; the first observations were the spiral or S-shaped nature of some filaments near sunspots seen in Hα and the rotation, or curved appearance, of sunspot fibrils (Hale, 1925). Nakagawa *et al.* (1971) explained the origin of these structures by describing the magnetic fields in the sunspot regions as twisted flux ropes. It was suggested that the direction of curvature of the fibrils was related to the sense of twist in the magnetic fields. For example, sunspots that appear to have rotated in a clockwise sense (*i.e.*, the fibrils bend away from the radial direction in a counterclockwise sense when going outwards) are formed in a flux rope with right-handed twist. From this, the idea that observations could be used to determine the sense of twist in the magnetic fields of active regions was established.

Soft X-ray (SXR) images of the corona taken during the *Skylab* and *Yohkoh* missions also revealed the occurrence of S-shaped structures. They are considered to result from enhanced dissipation that accumulates hot plasma along correspondingly shaped field lines. These structures were termed sigmoids by Rust and Kumar (1996) as a general designation for both forward and reverse S-shaped forms. Pevtsov (2002a) distinguished four sigmoid types: multiple loops, inter-region loops, single S-shaped loops, and interlocking (double-J) loops. However, it seems that single S-shaped and double J-shaped sigmoids on the one hand, and multiple-loop and inter-region loop sigmoids on the other, can be collectively referred to as *transient* and *long-lived* sigmoids, respectively. Transient sigmoids are sharp and bright, and associated with active regions; they frequently evolve into cusps or arcades of loops in association with an eruption. Long-lived sigmoids appear more diffuse. Similar sources have been discovered in the EUV (*e.g.*, Gibson *et al.*, 2002).

The occurrence of SXR sigmoids is correlated with a tendency of the active region to erupt into a coronal mass ejection (CME) (Canfield, Hudson, and McKenzie, 1999). This association can naturally be expected, since the curvature of the field lines producing the S shape is a signature of currents (free magnetic energy) in the corona and the emission itself is direct proof of locally enhanced heating (dissipation of free magnetic energy).

An important quantity in the study of twisted, current-carrying fields is the magnetic helicity: $H = \int \mathbf{A} \cdot \mathbf{B}\, \mathrm{d}^3x$, where $\mathbf{A}$ is the vector potential of the magnetic field $\mathbf{B}$. For cases where magnetic flux passes through the boundary of the volume being considered, for example solar active regions, the relative magnetic helicity H_r is to be used (Berger and Field, 1984). This is found by subtracting the helicity of a reference field (*e.g.*, a potential field) which has the same normal field at the boundary. Magnetic helicity is a global parameter of the considered volume and quantifies various aspects of the structure of the magnetic field and provides a common measure of topology between different flux systems (*e.g.*, Berger, 2000a, 2000b). For example, the twisted field in one region can be directly compared to the sheared field in another. For a magnetic flux rope the helicity is given by $H_\mathrm{r} = \Phi^2\,(Tw + Wr)$, where Φ is the axial magnetic flux within the rope, Tw is the number of windings of the field lines around the flux rope axis, and Wr is the writhe, which is a measure of the winding (or kinking) of the flux rope axis. In ideal MHD the magnetic flux and helicity are conserved (Woltjer, 1958); hence changes in the twist of the flux rope must lead to opposite changes of the writhe, a property that is relevant for our investigation.

A related quantity is the so-called force-free parameter α. Coronal active-region fields are assumed to be nearly force free (*i.e.*, they satisfy $\nabla \times \mathbf{B} = \alpha\mathbf{B}$ to a very good approximation). In general, α is a local parameter and varies across the field (but it is constant along the field lines). For linear force-free fields, characterised by uniform α, H_r and α are always of the same sign, and they are linearly related for small deviations from the potential state $\alpha = 0$

(Berger, 1985). Although vector magnetograms of active regions often reveal small-scale structures with varying magnitude and sign of α in the photosphere, one sign is normally dominant (Seehafer, 1990; Pevtsov, Canfield, and Metcalf, 1995; Hagino and Sakurai, 2004). Therefore, one sign of α and H_r, or a dominant chirality (handedness) of the magnetic field, can be associated with most active regions (with positive α and H_r corresponding to right-handed chirality). If a helical field with uniform sign of α contains a flux rope with little or no writhe, the sign of the twist in the rope equals the sign of α and H_r.

As we discuss in Section 2, all current sigmoid models involve a flux rope and they predict, or imply, a certain relationship between the orientation of the sigmoid, the writhe developed by the flux rope as it erupts, and the chirality of the field in which the sigmoid is formed. However, this relationship is not uniform among the models, so such observations can be used to provide a constraint. This is the goal of the present investigation.

The relationship between the orientation of the sigmoid and the dominant chirality of the active region field has been investigated by Pevtsov, Canfield, and McClymont (1997) and Burnette, Canfield, and Pevtsov (2004). It was found that in 90% of the cases studied forward (reverse) S sigmoids were formed in dominantly positive (negative) chirality regions. The remaining cases "tend to show patches of both signs of alpha in the photosphere" (Pevtsov, Canfield, and McClymont, 1997), suggesting that the sigmoids were formed in parts of the active region having a chirality sign opposite to the dominant one, so the relationship between the local sign of α and the sigmoid orientation may be universal.

Because we will check model predictions against this relationship, we cannot simply rely on this conjecture, despite its plausibility. Rather, we will consider several direct tracers of the erupting field's chirality (supplemented by the active region's dominant chirality, where available). The erupting field's chirality equals the chirality of the field in which the sigmoid is formed in all sigmoid models, save one (the reverse-shear model; Section 2.1).

We note that, since the correlation between chirality and S shape is so high, the observed moderate hemispheric preference of sigmoidal shape [forward (reverse) S in the southern (northern) hemisphere; Rust and Kumar, 1996] must be a consequence of the moderate hemispheric preference of the dominant chirality of active region fields [positive (negative) in the southern (northern) hemisphere].

The relationship between the sense of writhing, or kinking, of erupting flux ropes and their chirality is determined by helicity conservation to be such that – for rising flux ropes – the middle section of the flux rope takes a reverse (forward) S shape for positive (negative) chirality (Fan and Gibson, 2003; Kliem, Titov, and Török, 2004; see Section 2.2 for a detailed discussion). This is observable if the flux rope writhes sufficiently and contains filament material which traces its shape. The apex of rising filaments is then seen to rotate about the direction of ascent in a clockwise (counterclockwise) direction for positive (negative) chirality. The requirement of a clear apex rotation restricts our study to transient sigmoid events, which are most likely to be associated with the onset of CMEs. Multi-wavelength observations of sigmoidal active regions have shown that filaments are present in most (91%) cases (Pevtsov, 2002b). Not all of them erupt when a sigmoid brightens (Pevtsov, 2002b; Rust and Kumar, 1994), and the number of rotating erupting filaments is substantially smaller, but these provide a (small) sample of decisive tests.

The magnetic topology of filaments in the stable phase before eruption is a topic of considerable debate. Several groups favour a flux rope topology (*e.g.*, Priest, Hood, and Anzer, 1989; Priest, van Ballegooijen, and Mackay, 1996; Rust and Kumar, 1994; Aulanier and Démoulin, 1998; Amari *et al.*, 1999; Martens and Zwaan, 2001; Lionello *et al.*, 2002). A partially alternative model suggests that the supporting field largely possesses the topology of a sheared arcade. However, for large amounts of shear, magnetic reconnection produces a helical (flux rope) topology in the centre of the arcade, where the filament material

is expected to be trapped (DeVore and Antiochos, 2000). More importantly, the observations of erupting filaments suggest a flux rope topology after the onset of the eruption so clearly that it has become widely accepted for this phase (*e.g.*, Rust, 2003). This assumption is all we need for the present study. Indeed, it is strongly supported for our sample by the very fact that the filament rotates while erupting. The rotation is a consequence of the buildup of writhe, which for constant helicity must result from the conversion of twist (*i.e.*, in a flux rope topology).

In the present investigation we do not study the curvature of filaments prior to their eruption. The curvature at the filament ends is uniquely related to chirality, with filaments that make a forward (reverse) S shape at their ends having positive (negative) chirality (Rust and Martin, 1994). However, the middle section of the filament can have an uncorrelated curvature depending on the distribution of the vertical photospheric field in this region. We will consider the *change* of the orientation of the central section of erupting filaments as well as the orientation of sigmoidal sources, disregarding possible initial curvature in the middle section of the filaments.

We summarise sigmoid models and their predictions concerning S shape and chirality in Section 2, detail our data selection in Section 3, describe the determination of the chirality of the magnetic field in Section 4, analyse the data in Section 5, and conclude in Section 6.

2. Sigmoid Models and Simulations

2.1. Arcade Models

Perhaps the earliest model of sigmoidal coronal sources was put forward as part of the tether-cutting model for eruptive events (Moore and LaBonte, 1980; Moore and Roumeliotis, 1992; Moore *et al.*, 2001). This model suggests that self-amplifying ("runaway") magnetic reconnection occurs in the core of a sheared magnetic arcade, transforming part of the reconnected field lines into a twisted flux rope, which is then able to erupt as a result of the cut tethers. Prior to the eruption, the field lines in the strongly sheared core are aligned along the polarity inversion line in the middle and curve out to opposite sides at the ends, so appearing S or reverse-S shaped. The shape of the S is uniquely related to the sign of the shear and helicity in the arcade; a forward (reverse) S results in fields of positive (negative) helicity. The transient sigmoid results from enhanced dissipation at these field lines, owing to their reconnection. The flux rope has the same chirality as the original arcade, which implies a clockwise (counterclockwise) apex rotation for positive (negative) helicity (see Section 2.2 for a detailed discussion of apex rotation versus flux rope chirality).

An extension of the model was proposed by Kusano (2005) and will be referred to here as the reverse-shear model. If the inner part of a sheared arcade is subjected to shearing in the opposite direction and then perturbed, numerical experiments showed that the reconnection evolves in two phases. It commences in the basically horizontal shear-inversion layer on top of the inner arcade. After this reconnection has evolved sufficiently, a vertical current sheet is formed in the outer arcade above the shear inversion layer, and the subsequent evolution follows the tether-cutting and standard flare models (Kusano *et al.*, 2004). Sigmoidal field lines originating in the inner arcade and passing through current density enhancements in the shear inversion layer develop in the first reconnection phase. A forward (reverse) S results if the inner arcade has positive (negative) chirality, while the outer arcade and the flux rope formed within it have negative (positive) chirality. If the flux rope transforms some of its twist into writhe in the course of its rise (*i.e.*, if its apex rotates in photospheric projection),

then the constraint of helicity conservation requires that it rotates such as to align with the middle section of the sigmoid. This is an intrinsic property of the model, independent of the relationship between sigmoid shape and dominant chirality of the host active region. The latter depends on the question of whether it is the outer or the inner arcade that carries the major fraction of the active region's helicity. To comply with the correlation between dominant helicity and sigmoid shape found by Pevtsov, Canfield, and McClymont (1997), the model requires that the helicity of the host active region be mainly contained in the inner arcade.

However, to comply with the widely accepted view that CMEs represent the prime mechanism by which the Sun ejects the helicity of active region fields into interplanetary space (*e.g.*, Rust and Kumar, 1994; Low, 1996), the model requires that the helicity of the host active region be mainly contained in the outer arcade. Note that in our summary of sigmoid models in Table 1, we relate the sigmoid orientation and filament rotation to the chirality of the erupting field, which is the outer arcade for the reverse-shear model, independent of whether or not its chirality is the dominant chirality of the active region.

By construction, this model is applicable only to active regions that contain volumes of opposite helicity in sizable fractions. Following Rust and Kumar (1994) and Low (1996), we expect that the dominant helicity is typically contained in the erupting part of the field (*i.e.*, in the outer arcade). Then, the sigmoid orientation corresponds to the orientation found by Pevtsov, Canfield, and McClymont (1997) in the minority of cases, so that the reverse-shear sigmoid model by Kusano (2005) may be relevant for those, provided they conform to the assumed geometry of oppositely sheared arcades stacked on top of each other. When the model predictions are compared to observations of sigmoids formed in active regions that are clearly dominated by one chirality, disagreement must be expected and is indeed found (see Section 5).

2.2. Kink-Unstable Flux Ropes

Rust and Kumar (1996), hereafter RK, made an important step by suggesting that transient sigmoids result from an ideal MHD instability of a magnetic flux rope. They suggested the long-wavelength helical kink instability because it gives the flux rope an S shape when seen in projection onto the photosphere. The kink instability requires the flux rope twist to exceed a threshold value (*e.g.*, Török, Kliem, and Titov, 2004, and references therein) and facilitates the development of a clear S. The idea of sigmoids being part of a kinked flux rope was supported by estimating the deformation of the kinked rope, which gave values consistent with the range observed for sigmoids. Observations of filament eruptions that strongly suggest a helical kink occurring in flux rope topology were presented, *e.g.*, by Ji *et al.* (2003), Rust and LaBonte (2005), and Williams *et al.* (2005).

However, a number of sigmoid properties appear to be incompatible with the model. The most essential one for the present investigation is the relationship between the sense of the S-shaped rope and the chirality of the field. To be in accordance with the conclusion of Nakagawa *et al.* (1971), RK propose that a positive (negative) chirality kink-unstable flux rope produces a forward (reverse) S shape, implying a counterclockwise (clockwise) rotation of the flux rope apex upon deformation.

The energy reservoir of the helical kink lies in the twist of the field about the magnetic axis of the rope. Part of the twist is transformed into writhe of the axis as the instability develops. The conservation of helicity in ideal MHD requires the resulting writhe to be of the same sign as the transformed twist. This means that an initially straight flux rope axis turns into a helix of the same handedness as the twist of the field lines about the axis. Seen

in projection, those parts of the flux rope axis moving towards an observer (moving upwards on the Sun) approach the shape that the field lines running over the axis initially had, while the parts moving away from the observer (downwards on the Sun) approach the shape that the field lines running under the axis initially had. Therefore, the apex of an upward kinking flux rope with right-handed (left-handed) twist rotates clockwise (counterclockwise) in projection while rising, to yield a reverse (forward) S shape of the kinked rope axis, and the opposite apex rotation and axis shape result if the apex of the flux rope moves downwards during the instability (Kliem, Titov, and Török, 2004).

A caveat is in order here that applies if the flux rope remains at a very low height and has no dip. Berger and Prior (2006) have recently shown that a curve (*e.g.*, the axis of a flux rope), anchored at both ends in the same plane, with positive (negative) writhe can exhibit a forward (reverse) S shape, if the apex height is less than roughly 0.4 times the footpoint separation. This situation is, however, not relevant for the evolved phase of solar eruptions we focus on in the present study.

The RK model leaves open the possibility that a correctly orientated sigmoid could be formed by the flux rope if it undergoes a downward kink, that is, if the flux rope forms a dip at the centre. In this case an S shape would be produced that is in line with the sigmoid observations. However, because the majority of transient sigmoids evolve into long-lasting arcades or diffuse structures, which are the SXR signatures of eruptive flares and CMEs, they must involve an upward motion of the unstable current-carrying field. This means that the association between chirality and S shape *implied* by the model for upward-kinking events is in fact opposite to the association observed for sigmoids.

Furthermore, several simple geometrical properties of sigmoids are difficult to reconcile with the RK model. Transient sigmoids are typically observed to be sharp and narrow in their middle section but taper off diffusively at their ends, opposite to the behaviour expected for a rising flux rope whose end points are tied in the photosphere and whose top part expands. Some sigmoids appear to be split into two symmetric J's, which resemble an S only collectively, and the end points of some sigmoids appear to move apart during the brightening (Manoharan *et al.*, 1996). Many transient sigmoids, including the one shown in RK, appear to include multiple threads, some of which spread off of the main trace of the sigmoid in its bright middle part. To the best of our knowledge, neither rotation nor upward expansion of the middle section of transient sigmoids in the course of their brightening, which is expected for a kinking and rising loop seen in projection, has so far been reported.

This picture of sigmoids being part of a kinked flux rope represents the way the model was introduced in RK as well as its predominant perception in the literature. However, RK also suggested the possibility that the sigmoids are merely associated with kinked flux ropes but not really contained in them: "[A]lthough the filamentary flux tubes erupt into space…, their solar epitaphs are S's etched into the corona." This points already to some elements in the Titov and Démoulin model, which we discuss next, and this interpretation of the RK model shares the good agreement of that model with the observed orientations of sigmoids.

2.3. Current Layer or Sheet Driven by a Flux Rope

Titov and Démoulin (1999) and Titov, Démoulin, and Hornig (1999) combined the elements of unstable flux ropes and layers of enhanced current density in two variants of a new sigmoid model. They suggested that transient sigmoidal brightenings are triggered by an ideal MHD instability or a catastrophe of a flux rope, but that the sigmoid forms in a current layer steepened below the unstable flux rope. A current layer in a separatrix surface formed by bald-patch field lines (BPSS) was suggested in Titov and Démoulin (1999) (see also Low

and Berger, 2003). The bald-patch field lines and the surface they form touch the photosphere tangentially at the polarity-inversion line. They exist prior to the instability, but only the dynamic evolution of the flux rope causes the current density and dissipation in the BPSS to rise sufficiently so that a bright, transient sigmoid forms. A vertical current layer, steepening and extending in the wake of the rising flux rope, was suggested in Titov, Démoulin, and Hornig (1999). This is topologically similar to the standard flare model (*e.g.*, Shibata, 1998) and the tether-cutting model. In this variant of the model, the current layer has its seed in a preexisting so-called hyperbolic flux tube (HFT) below the twisted, current-carrying flux rope. The HFT is a generalisation of an X-type magnetic topology in three dimensions. It can be current-free initially, but it is unstable to collapse into a layer of exponentially rising current density (a true current sheet) upon external perturbations (Titov, Galsgaard, and Neukirch, 2003).

It is possible that both variants of the model are realised in sigmoids, depending on whether the pre-eruptive configuration includes a BPSS or an HFT. The BPSS version has the advantage of offering a possible explanation also for long-lived sigmoids, for which the current density in the BPSS may be only moderately enhanced under the influence of the more gradual evolution of the host active region (Gibson *et al.*, 2004). Since the field lines passing through the current layer run significantly below the magnetic axis of the flux rope, they show a forward (reverse) S shape in projection for positive (negative) chirality of the flux rope field for any direction of the flux rope displacement in both variants of the model and in agreement with sigmoid observations.

Numerical simulations of dynamically evolving flux ropes have independently confirmed both variants of the Titov and Démoulin model. Fan and Gibson (2003, 2004), and Gibson *et al.* (2004) followed the evolution of a flux rope emerging through the bottom boundary of their simulation box into a preexisting magnetic arcade, using boundary conditions that implied the presence of a BPSS from the emergence of the magnetic flux rope axis until the end of the simulation. After the twist in the emerged part of the flux rope exceeded $\approx 3.5\pi$, the helical kink instability occurred and a sigmoidal layer of strongly enhanced current density was formed in the BPSS. The section of the BPSS under the flux rope apex collapsed to form a narrow trace, as is typical of the middle section of transient sigmoids, and it was orientated according to the observed sigmoid – chirality association. In agreement with the conservation of the total helicity in the box, the writhe of the kinked flux rope grew such that it developed an S shape opposite to the S shape of the BPSS.

Kliem, Titov, and Török (2004), Török, Kliem, and Titov (2004), and Török and Kliem (2005) used the flux rope equilibrium by Titov and Démoulin (1999) as the initial condition, choosing the parameters such that the flux rope had supercritical twist for the occurrence of the helical kink (again, twist $\gtrsim 3.5\pi$) and that an HFT was present below the rope. Depending on the detailed parameter settings, upward or downward kinking occurred spontaneously. The upward-kinking flux rope caused the HFT to collapse into a vertical current sheet threaded by sigmoidal field lines, with the sense of the S shape as observed for sigmoids: forward (reverse) S for positive (negative) twist in the rope. Again, the conservation of helicity caused the apex of the upward-kinking flux rope to rotate such that the rope developed the opposite S shape.

In both series of simulations, the current density in the formed current sheet was observed to exceed the current density in the flux rope after the kink instability had developed. Hence, in agreement with the suggestion in Titov and Démoulin (1999), enhanced dissipation and the formation of a bright SXR or EUV source are to be expected preferentially for the sigmoidal field lines which thread this current sheet. It seems that precisely this situation has been observed by *Yohkoh* in the eruptive M flare and sigmoid event on 19 October 1994,

discussed in Moore *et al.* (2001); a bright, stationary sigmoid and a much fainter rising loop rooted in the two crooks of the sigmoid were seen. The series of simulations by the two groups immediately reproduced most of the geometrical sigmoid properties mentioned here, which are difficult to reconcile with the suggestion that sigmoids are part of kinking flux ropes; see Gibson *et al.* (2006).

The ideal MHD instability of the flux rope is not restricted to the helical kink. Titov and Démoulin (1999) also mentioned an expansion instability of the major radius of the partial torus that is formed by the flux rope. This torus instability was shown to reproduce some of the essential properties of CMEs (Kliem and Török, 2006; Török and Kliem, 2007). Numerical simulations of the torus instability indeed confirm the steepening of a sigmoidal current layer below the rising flux rope and a transformation of flux rope twist into writhe, that is, opposite S shapes of current layer and rope, similar to the helical kink. If values of the twist below the threshold of the helical kink instability are chosen to separate the torus instability from the helical kink, then the resulting writhe (apex rotation) remains smaller than in the simulations of the kink instability.

2.4. Vortex-Driven Model

Finally, we summarise the simulations of coronal flux ropes twisted by photospheric vortices (Amari *et al.*, 1996; Török and Kliem, 2003; Aulanier, Démoulin, and Grappin, 2005). It was found that part of the injected twist is transformed into writhe of the flux rope axis. This occurred from the beginning of the simulations (which started from a potential configuration with vanishing helicity), that is, for any amount of the injected twist. Analogous to the case of the kink instability, positive (negative) twist was transformed into writhe of the same sign so that the apex of the formed flux rope rotated clockwise (counterclockwise) while rising, to give the magnetic axis a reverse (forward) S shape. This is opposite to the observed association of sigmoid shape with chirality. However, a vertical current layer formed below the flux rope with a projected S shape opposite to that of the rope axis (*i.e.*, in agreement with the observed sigmoid shape). Because the rotation of photospheric flux concentrations typically have time scales of days (Brown *et al.*, 2003), these simulations are probably relevant for long-lived sigmoids only.

2.5. Summary of Models

It is obvious that *i*) sigmoidal field lines are associated with magnetic flux ropes in all of the models; *ii*) the observed preferred association between sigmoid shape and chirality of the field (Pevtsov, Canfield, and McClymont, 1997) requires the sigmoid to have the same orientation as the field lines that run *below* the magnetic axis of the rope; *iii*) the conservation of magnetic helicity forces the magnetic axis of a rising and writhing flux rope to approach the shape of the field lines *above* the axis; and *iv*) layers or sheets of enhanced current density consistent with the observed sigmoid orientation are available in all models (although a different current layer was suggested as the site of the sigmoid in Kusano, 2005).

Table 1 summarises the different predicted or implied relationships between the chirality of the erupting field, the orientation of the sigmoid, and the rotation of the flux rope apex in photospheric projection. Note that we have listed the *implied* relationships for the standard interpretation of the RK model (not the ones suggested in their paper) and that the chirality of the field in which the sigmoid is formed equals the chirality of the erupting field in all models, save the reverse-shear model.

Table 1 Model predictions for the relationship between chirality (or sign of helicity H_r) of the erupting field, sigmoid shape, and projected flux rope (FR) apex rotation for right-handed chirality and upward moving flux ropes.

Model	H_r	Sigmoid shape	FR apex rotation
TC[a]	> 0	S	*CW*
Reversed shear[b]	> 0	Z	*CW*
RK[c]	> 0	*Z*	*CW*
TD[d]	> 0	S	*CW*
Vortex[e]	> 0	S	CW

[a]Tether cutting model, *e.g.*, Moore *et al.* (2001). [b]Kusano (2005). [c]Rust and Kumar (1996). [d]Titov and Démoulin (1999) and Titov, Démoulin, and Hornig (1999). [e]Amari *et al.* (1996), Török and Kliem (2003), and Aulanier, Démoulin, and Grappin (2005). Entries typeset in italics are *implied* by the models; other entries are the predicted ones. All entries in columns 3 and 4 flip if the chirality is reversed to $H_r < 0$. The RK model yields an S shape and CCW rotation of the flux rope in the case of a downward kink, which is unlikely to be associated with CMEs.

3. Data Selection and Instrument Description

Events which would be suitable for this study were initially sought by using previous identifications of SXR sigmoids reported in the literature and also observations of filaments that rotate upon eruption from the TRACE data catalogue. For the final data selection it was required that the direction of filament rotation could be determined unambiguously. This limited the number of events found in the period 1996 – 2003 to a small sample, which is completely included in the analysis of this paper. A suitable case of a sigmoid observation in the EUV and a filament eruption that has been successfully reproduced in a numerical simulation of a kink-unstable flux rope were also included.

3.1. *Transition Region and Coronal Explorer*

The *Transition Region and Coronal Explorer* (TRACE; Handy *et al.*, 1999) images the photosphere, transition region, and corona covering a temperature range from 6000 K to 10 MK. Images from TRACE are used to study the evolution of active region filaments and their motions upon eruption. As well as the filament evolution, flare ribbons can also be studied using the 1600 Å and 1700 Å wavelength bands, which image plasma at temperatures between 4000 and 10 000 K. The 195 Å and 171 Å wavebands image plasma in the temperature ranges $(5 – 20) \times 10^5$ K and $(1.6 – 20) \times 10^5$ K, respectively. These wavebands are used to study the filament in absorption and in emission if heating occurs during eruption, and also to reveal the formation of a sigmoid in one event.

3.2. Michelson Doppler Imager

The photospheric magnetic-field evolution is studied by using data from the Michelson Doppler Imager (MDI; Scherrer *et al.*, 2005) onboard the *Solar and Heliospheric Observatory* (SOHO). MDI measures the line-of-sight magnetic field in the mid-photosphere. Full-disc magnetograms (the average of five magnetograms) with a 96-minute cadence were used in this work. To study the magnetic evolution across the entire solar disc, all data are differentially rotated to the time of central meridian passage. This corrects for the area foreshortening observed in the data when active regions are close to the solar limb and eases the interpretation of the magnetic structure.

3.3. *Yohkoh* Soft X-Ray Telescope

The Soft X-ray Telescope (SXT) onboard *Yohkoh* (Tsuneta *et al.*, 1991) is used to follow the evolution of structures in the corona. SXT was a grazing incidence telescope which formed X-ray images in the 0.25- to 4.0-keV energy range, which corresponds to a wavelength range of 3 – 60 Å. Full-disc and partial frame SXT data are used in this work, in particular data taken with the Dagwood (AlMg) filter.

3.4. Ground-based Hα and Vector Magnetograph Data

Ground-based data were used to obtain information on the evolution of the filaments observed in the light of Hα (6563 Å). Data were obtained from the Big Bear Solar Observatory (BBSO) and the Holloman Observatory, which forms part of the SOONSPOT network. The Singer telescope at BBSO produces full-Sun images at a cadence of roughly one minute and pixel size $1'' \times 1''$. Partial-Sun images from the SOON-FMQ7 telescope at Holloman were used; these have a pixel size of $0.781'' \times 0.781''$ and 30-second cadence from five minutes prior to the flare onset until the peak of the flare, and five-minute cadence thereafter. Vector magnetograph data were obtained from the NASA Marshall Space Flight Center and from the Mees Solar Observatory.

4. Determination of Field Chirality

Because it is impossible to measure the three-dimensional coronal magnetic field structure, assumptions enter all determinations of the helicity it contains. There are various methods to estimate H_r, and so the results can often be mutually supported by employing more than one of them. We are interested only in the sign of the helicity, the chirality of the field, and therefore do not need to use the most elaborate approach of calculating the helicity integral from an extrapolated nonlinear force-free field. Rather, for the two active regions where a vector magnetogram is available, we determine the value of α of the linear force-free field that best matches the observed field components in the plane of the magnetogram. This "alpha-best" method, which yields the dominant chirality of the active region, was also used by Pevtsov, Canfield, and McClymont (1997) and Burnette, Canfield, and Pevtsov (2004). For both active regions the absolute value of the obtained α_{best} equals the maximum value permitted by the magnetogram size. We therefore consider the sign of α_{best} to be reliable in spite of the substantial intrinsic scatter of the method (Kliem and Valori, private communication). For a third active region, the sign of α in the area of the filament eruption and sigmoid formation was determined from the vector magnetogram in Song *et al.* (2002).

In addition, we use proxies of the chirality. "Magnetic tongues"; low coronal or chromospheric brightenings; and filament fine structure, end shape, and magnetic connectivity are the three categories of proxies employed. They are introduced in the following. The latter two refer directly to the erupting part of the active region's field and are, therefore, superior to the α_{best} value for our purposes.

Observations of the longitudinal magnetic field component can be used to infer the sign of twist in emerging flux ropes, just as the apex of the Ω loop is crossing the photosphere. The presence of twist produces a contribution of the azimuthal field component projected on to the line-of-sight magnetic field which is measured by, for example, MDI onboard SOHO. Observationally this is seen as an elongation of the polarities or "tongues" in the MDI data (López Fuentes *et al.*, 2000). For positive twist the leading polarity extends under the south side of the following polarity and for negative twist it is the mirror image.

For a flux rope topology, Démoulin, Priest, and Lonie (1996) have shown that the footprints of quasi-separatrix layers (QSLs) form two J or reverse-J shapes and their orientation and displacement along the polarity inversion line reflect the sign of twist in the rope. On eruption, magnetic energy dissipation occurs primarily along, or in the vicinity of, the QSLs and the observational signature of this energy release is seen as a brightening of the two J's as flare ribbons. Two J shapes together forming a reverse S indicate negative twist and J shapes forming a forward S indicate positive twist. This association is identical to the one in the Titov and Démoulin sigmoid model, and indeed, in their model the sigmoid and the flare ribbons brighten at the same QSL (which is also true for the tether-cutting model). However, this is not true for the other sigmoid models discussed in Section 2. By using this proxy of the chirality for several active regions of our sample, we are not making any assumption about the nature of the sigmoid in the coronal volume above the ribbons!

The displacement of the flare ribbons along the polarity inversion line in the early phase of an eruption reflects the chirality of the field also in an arcade topology. The direction of this displacement is identical to the case of a flux rope studied by Démoulin, Priest, and Lonie (1996); if the polarity inversion line is (rotated to be) vertical on the solar image, the left ribbon is displaced downwards and the right ribbon is displaced upwards for positive chirality, the displacements reversing when the chirality is opposite.

Martin, Billimoria, and Tracadas (1994) suggested that the structural properties of filaments could be uniquely related to the chirality of the field in which the filaments are contained. Work by Rust and Kumar (1994), Chae (2000), Aulanier, Srivastava, and Martin (2000), and Ruzmaikin, Martin, and Hu (2003) has shown that "sinistral" ("dextral") filaments form in fields of positive (negative) chirality. Whether the filament belongs to the "sinistral" or "dextral" category can be determined from properties such as the magnetic connection of the filament ends, the orientation of the Hα fibrils in the filament channel, or the orientation of the filament barbs (*e.g.*, Martin, 1998). Studying filaments at EUV wavelengths also allows the investigation of chirality from the way in which emitting and absorbing filament threads are twisted about each other (Chae, 2000).

For each active region in our sample, more than one method of chirality determination is available. They all yield the same results (Section 5). This indicates a largely uniform chirality for the three active regions for which the local and global chiralities were determined (events on 7 April 1997, 19 July 2000, and 27 May 2002). A similar situation is indicated, albeit less clearly, for two further active regions of our sample. One was a relatively simple bipolar region, not dominated by the emergence of multiple structures (event on 12 May 1997). A predominantly uniform sign of α was reported for the other (event on 6 June 2000) (Song *et al.*, 2002). However for the event on 15 June 2001 the injection of helicity changed sign prior to the eruption (Romano, Contarino, and Zuccarello, 2005), so the active region may have contained both chiralities in sizable fractions. Whether the complex of active regions that produced the 2 May 2003 event was dominated by uniform or a mixture of chiralities is not known.

5. Results

5.1. 7 April 1997

Southern hemisphere NOAA active region 8027 produced a filament eruption on 7 April 1997 and a C6.8 GOES class flare beginning just after 13:50 UT. The event triggered a fast (≈ 900 km s^{-1}) halo CME. A forward-S sigmoid was observed in the region by 06:00 UT,

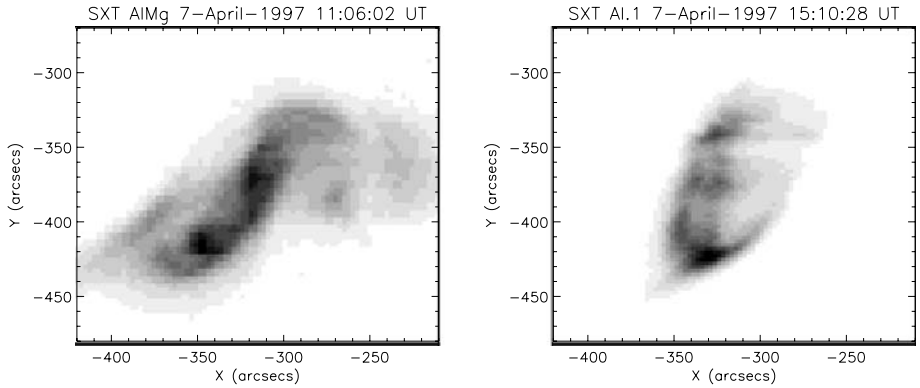

Figure 1 Reverse colour table soft X-ray images of the 7 April 1997 event in active region 8027 from *Yohkoh*/SXT. The sigmoid to cusp transition is clearly seen. The second image is aligned to the time of the first image.

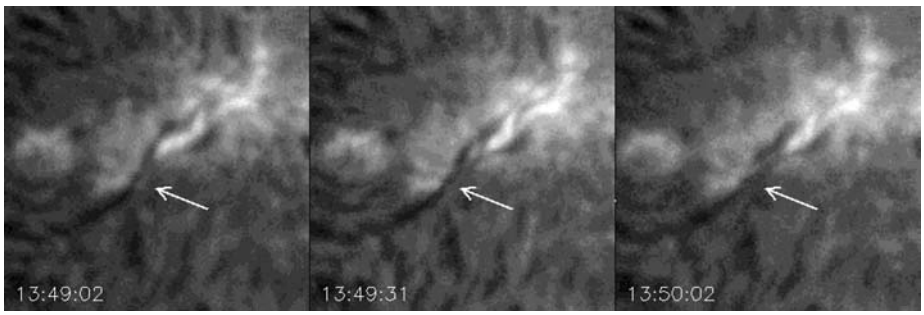

Figure 2 SOONSPOT Hα images of the 7 April 1997 event in active region 8027 showing the clockwise rotation of the filament at the location of the arrow. The field of view of each image is $117'' \times 117''$.

which became brighter and more defined and then evolved to a cusp after eruption, as seen in SXT data (Figure 1). The onset of the eruption was missed by *Yohkoh,* which was in spacecraft night from 13:30 to 14:10 UT, so the evolution at the time of the filament activation and flare onset cannot be studied in soft X-rays. The Hα data show the filament rotation beginning at 13:50 UT with a clockwise rotation of the filament axis (Figure 2). These data also show the formation of clear flare ribbons during the eruption which form a forward-S shape and diverge as the flare progresses (not included in the figure). The photospheric magnetic fields were followed during the whole disc passage of the active region, which was seen to have a bipolar classification. Magnetic "tongues" were present in the region when it was emerging close to the east limb. Later in the evolution of the region, a rapid decay of the flux can be seen as the polarities approach each other and cancel (Figure 3).

The tongues show that the leading negative polarity extends along the south side of the following positive polarity, indicating the presence of positive helicity. The magnetic connectivity of the filament indicates that it belongs to the sinistral category and therefore had positive chirality. We conclude from the MDI tongues, orientation of the flare ribbons, and sinistral classification that this active region as a whole, and the erupting field in particular, had positive helicity.

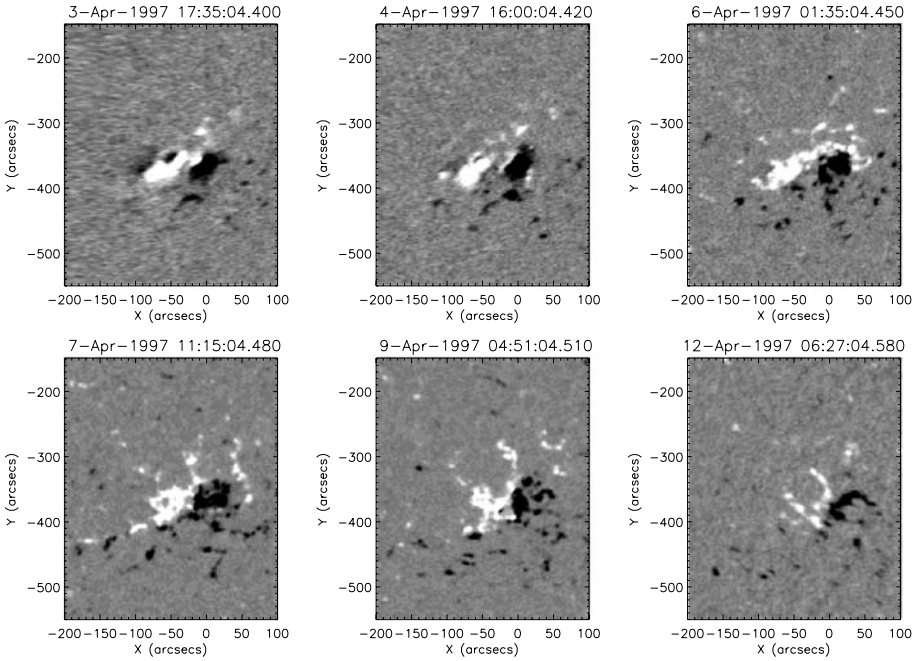

Figure 3 MDI data showing active region 8027, which produced the filament eruption on 7 April 1997. All images are rotated to the time of central meridian passage and have been corrected for area foreshortening. The first image shows the presence of "tongues" (where the leading negative polarity extends under the trailing polarity), which indicate the presence of positive helicity.

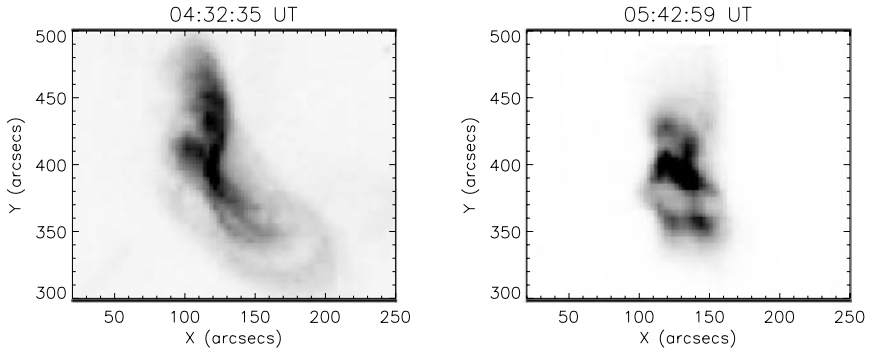

Figure 4 Partial frame images of active region 8038 on 12 May 1997 taken by the Soft X-ray Telescope on *Yohkoh* showing sigmoid to arcade transition.

5.2. 12 May 1997

Northern hemisphere NOAA active region 8038 erupted on 12 May 1997 and underwent a sigmoid to arcade transition before and after the filament eruption (Figure 4). The sigmoid had a reverse-S orientation. A GOES C1.3 class flare associated with the filament eruption took place in the active region, beginning at 04:42 UT. *Yohkoh* entered spacecraft night at 04:35 UT and so was unable to observe the eruption onset. An Hα filament was observed

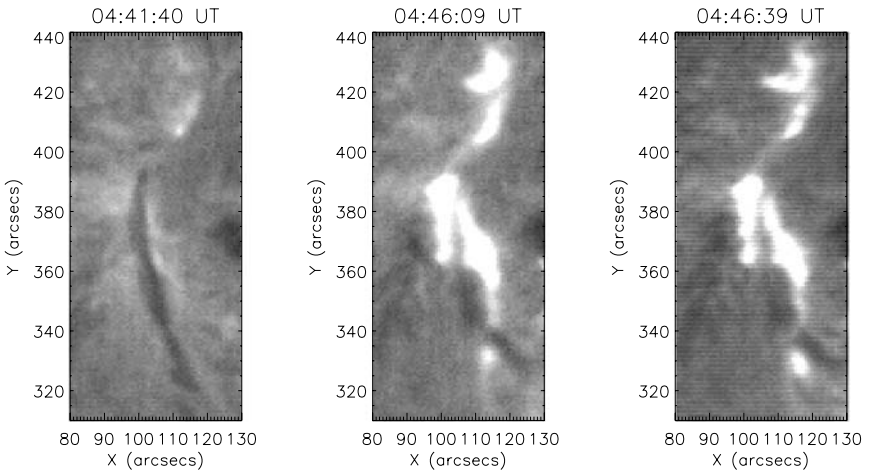

Figure 5 SOONSPOT Hα images of active region 8038 on 12 May 1997 showing the formation of flare ribbons, which collectively form a reverse S, and the counterclockwise rotation of the filament.

in the active region and was orientated almost North – South along the polarity inversion line. As the filament started to erupt its axis rotated counterclockwise (Figure 5). Further evidence to support the rotation of the filament is seen in the interplanetary medium. Webb *et al.* (2000) noted that the filament rotated upon eruption, changing from a North – South to East – West orientation, and the new East – West orientation was still held by the flux rope at one AU. This has been confirmed by Attrill *et al.* (2006). The active region was bipolar with a compact positive leading polarity and dispersed negative trailing polarity. Convergence of the opposite polarities occurs during the two days leading up to the eruption. The magnetic connectivity of the filament was such that it has a dextral classification, suggesting negative chirality.

At the time of the flare two bright ribbons start to form, as seen in the Hα data (Figure 5). The ribbons are displaced along the polarity inversion line, they are reverse J in shape or, if viewed together, form a reverse S, and they appear spatially coincident with the location of the soft X-ray sigmoid. The displacement and orientation of the flare ribbons and the dextral filament classification indicate that the magnetic field involved in the eruption contained negative helicity.

5.3. 6 June 2000

On 6 June 2000, northern hemisphere NOAA active region 9026 produced a failed filament eruption followed by two successful eruptions within two hours. The failed eruption took place between 13:30 and 13:45 UT and was accompanied by a GOES X1.1 class flare. A reverse-S sigmoid became visible at the start of the failed eruption. This then brightened at the end of the failed eruption and the onset of the first successful eruption (Figure 6), which reached GOES class X2.3 at 15:25 UT, and started with the eruption of another section of the extended filament channel. Neither a clear filament rotation nor a new sigmoid appeared in the successful eruption.

At the start of the failed eruption a helical brightening is observed to wrap once about the body of the filament in a way that suggests left-handed chirality. Then, a counterclockwise rotation of the filament body followed by a shredding of the filament is observed (Figure 7).

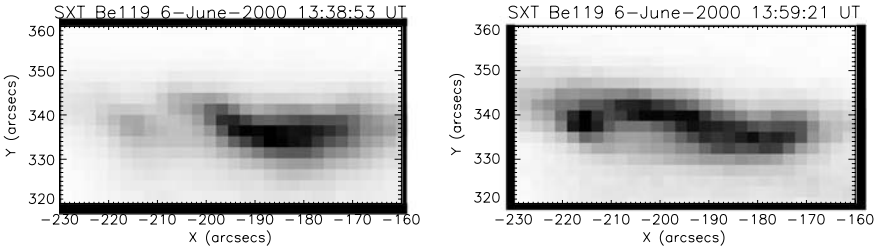

Figure 6 Soft X-ray image of the reverse-S sigmoid in active region 9026 on 6 June 2000.

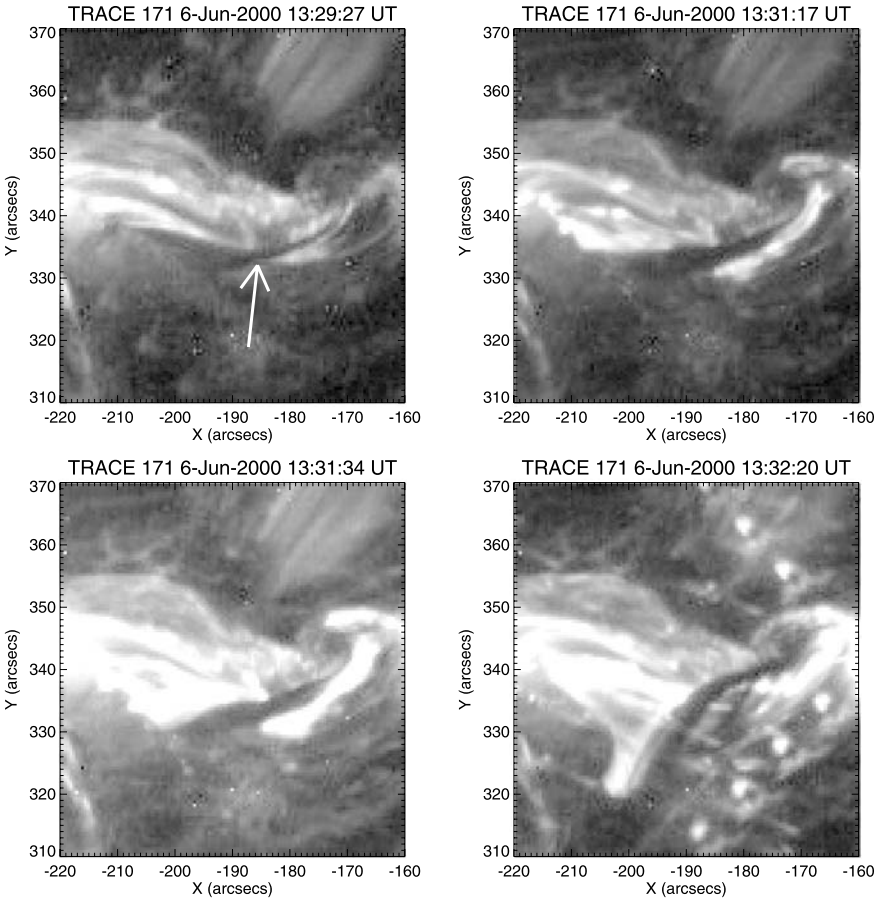

Figure 7 TRACE 171 Å images showing the counterclockwise rotation of the erupting but non-ejective filament on 6 June 2000 in active region 9026. The arrow marks the initial position of the filament.

Simulations of kink-unstable flux ropes by Török and Kliem (2005) have shown that such shredding occurs when a current sheet is formed above the flux rope and subsequent reconnection causes the top part of the flux rope to expand sideways. The magnetic connectivity of the filament is consistent with a dextral classification. The MDI data show a quadrupolar

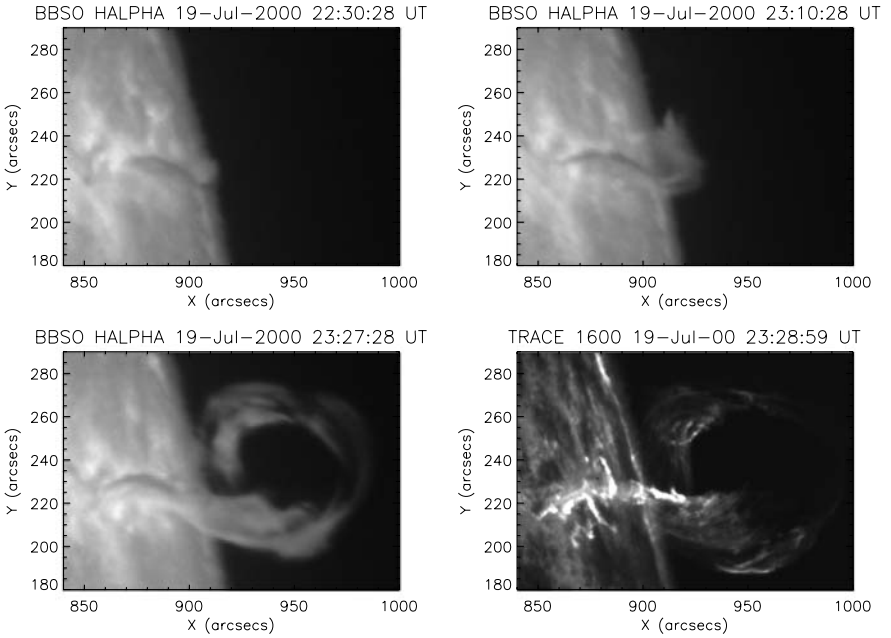

Figure 8 Big Bear Solar Observatory Hα images of active region 9077 on 19 July 2000 showing the counterclockwise rotation of the filament. The TRACE 1600 Å image shows the formation of flare ribbons which form a reverse-S shape and indicate negative helicity.

region that had already emerged when first visible on the solar disc. The magnetic polarities are seen to converge in the time leading up to the eruption, and flux cancellation occurs throughout the disc transit. This region was the focus of a study by Song *et al.* (2002), who used vector magnetograph data to determine the sign of α from the current helicity density $J_z B_z = \alpha B_z^2$ in the region of the failed filament eruption. They found that α was dominantly negative (see their Figure 8) and that the transverse component of the vector field in the negative polarity rotated counterclockwise, indicating negative twist. We conclude from the dextral classification of the filament and negative α and twist observations that the helicity sign of the field involved in the eruption is negative.

5.4. 19 July 2000

On 19 July 2000, northern hemisphere NOAA active region 9077 produced a failed filament eruption as it approached the west limb. Owing to the location of the active region close to the solar limb, soft X-ray data cannot be used to search for the presence of a sigmoid. However, on 14 July 2000 when the region was closer to the central meridian, a reverse-S sigmoid was observed (see Figure 10 in Zhang, 2006). Data from the TRACE spacecraft and Big Bear Solar Observatory show that the filament eruption on 19 July 2000 started at approximately 23:10 UT and that the filament axis rotated in the counterclockwise direction (Figure 8). No soft X-ray flare accompanied this event; however, TRACE 1600 Å data show the formation of ribbons which are clearly seen by 23:30 UT. The shape of the ribbons are that of two reverse J's, which together form a reverse S shape (Figure 8).

Rust and LaBonte (2005) investigated this eruption and from studying the deformation of the filament axis and the absorbing and emitting threads making up the filament they

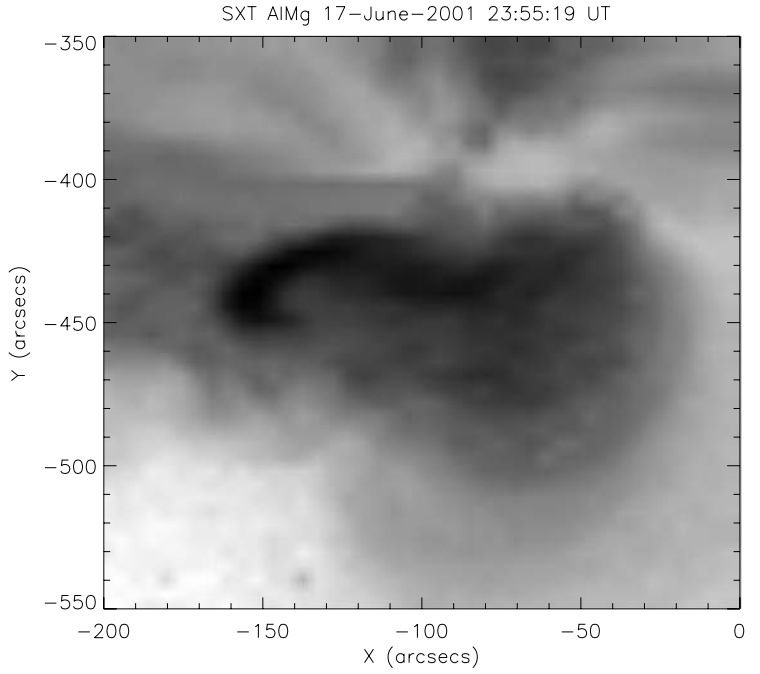

Figure 9 Soft X-ray image of active region 9502 on 17 June 2001 showing the reverse-S sigmoid.

assigned positive twist and writhe to the filament upon eruption (see their Figure 2). This means that the filament axis rotated clockwise. However, the image in their paper is actually the mirror image of the original, so the correct rotation of the filament axis is in fact counterclockwise and the correct twist and writhe signs should be negative (see also Romano, Contarino, and Zuccarello, 2003). MDI data indicate that active region 9077 was a complex multipolar region which showed motions, including convergence along the polarity inversion line on which the filament lies, and much cancellation of the magnetic field.

We find that the helicity sign in active region 9077 is negative from the shape of the TRACE ribbons and from the sign of $\alpha_{\rm best}$ (< 0), determined from a Mees Observatory vector magnetogram of the active region taken on 14 July 2000 after the Bastille Day flare. This agrees with the detailed analysis of vector magnetograph data from the region by Zhang (2002).

5.5. 15 June 2001

On 15 June 2001, the southern hemisphere NOAA active region 9502 produced a filament eruption associated with a GOES M6.3 flare and a fast (≈ 1100 km s^{-1}) CME. There is no observation of a sigmoid in this active region during the time *Yohkoh* was observing on this day. However, the eruption took place during a time period when the satellite was in spacecraft night. A reverse-S sigmoid was observed in the region on 17 June 2001 (Figure 9) two days after the eruption and when the active region was closer to the central meridian. TRACE observed the eruption through the 195 Å waveband and observed that the axis of the filament rotated counterclockwise. The TRACE data also show the formation of J-shaped flare ribbons, which together form a reverse S; these were clearly observed by 10:07 UT

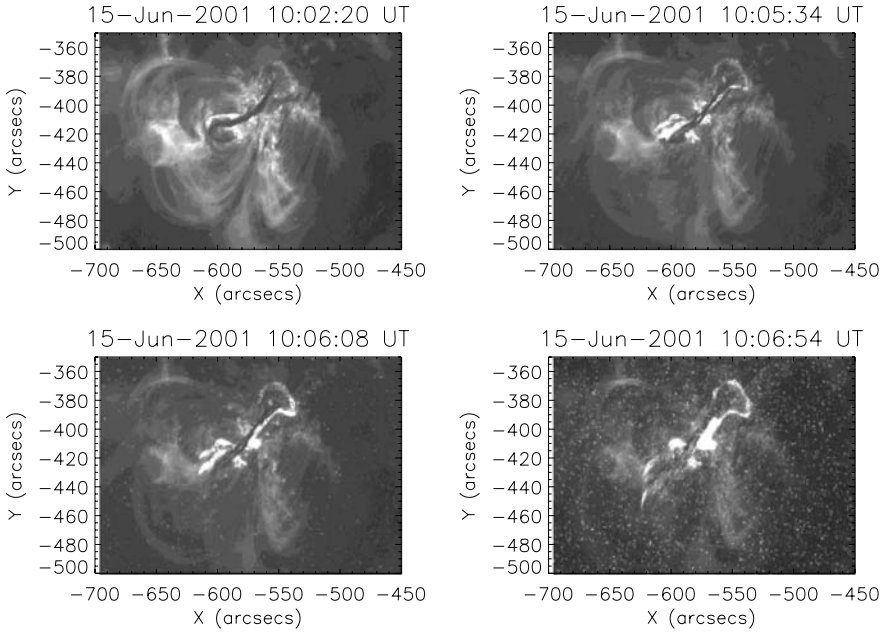

Figure 10 TRACE 171 Å waveband images of active region 9502 on 15 June 2001 showing the counter-clockwise rotation of the filament upon eruption and the formation of flare ribbons.

(Figure 10). The MDI data show that active region 9502 was a bipolar region with negative leading polarity. Monitoring the evolution across the solar disc shows that the flux in both polarities disperses rapidly and the two polarities cancel with each other. The magnetic connectivity of the filament is consistent with a dextral classification.

From the observation of the reverse-S flare ribbons and the filament's dextral class we conclude that the helicity sign of the erupting field is negative. Romano, Contarino, and Zuccarello (2005) also studied the MDI data in relation to this filament eruption and concluded that the footpoints of the magnetic field lines in the photosphere first imparted positive helicity over a period of ≈ 4 hours but then imparted about twice the amount of negative helicity into the filament in the ≈ 2.5 hours preceding and including the eruption. However, this work does not study the sign of helicity already contained in the coronal field, only that being injected by footpoint motions.

5.6. 2 May 2003

On 2 May 2003, NOAA active region 10345 produced a failed filament eruption which was associated with a M1.0 GOES class flare beginning just after 02:47 UT. Hα data show that the initial shape of the filament is that of a forward S orientated along the East – West aligned neutral line (Figure 11). Just prior to the eruption the eastern end of the filament lengthens (to the North) as the filament channel darkens towards the growing NOAA active region 10349. The result of this extension is that the filament has two "arms": the original East – West orientated arm in the core of AR 10345 and a curved North – South orientated arm whose northernmost part extends to the east into the periphery of the leading spot of AR 10349. Overall, the resulting long filament had a slightly reverse-S shape just prior to eruption (Figure 12a).

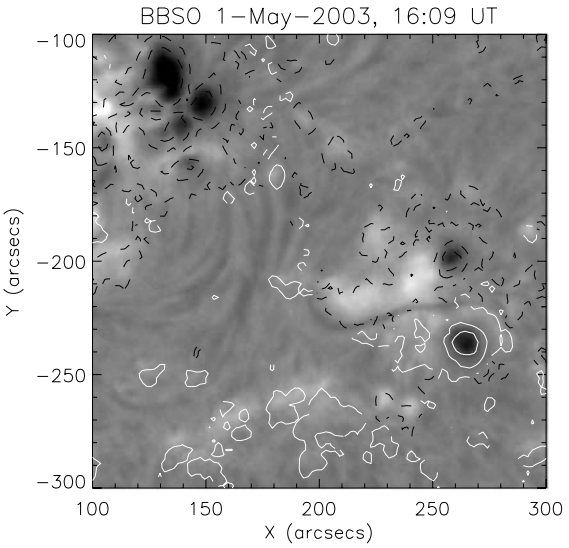

Figure 11 Big Bear Solar Observatory Hα image of the filament in active region 10345 (centre right area of the image) overlaid with MDI flux density contours. White continuous (black broken) lines represent contours set at positive (negative) flux densities of ± 50, 500, and 1000 G. Active region 10349 is visible in the top left part of the image.

There are several pieces of evidence showing that this filament had right-handed helicity. The clearest is a brightening at the beginning of the eruption which propagated outwards in both directions from a position under the middle of the East – West arm of the filament. The western part of the brightening emerged from the northern side of the filament, while the eastern part of the brightening emerged from its southern side. The eastern part was wound about the eastern edge of the original East – West filament section such that it crossed over the absorbing material in the filament body to extend to the North. These two brightenings indicate a twisted magnetic field with nearly a full turn along the East – West filament section (Figures 12b and 12c). The northward extension indicates a smaller amount of twist in this section of the filament. Second, the magnetic connections of the filament ends, both of the original East – West section (Figure 11) and of the whole erupting filament (Figure 12a), show that it belongs to the sinistral classification. This is particularly clear after the filament increased in length, when it extends from the periphery of the positive polarity spot in AR 10345 to the periphery of the negative polarity spot in AR 10349. Third, the end sections of the original East – West filament had a shape corresponding to an S, which is characteristic of sinistral filaments (Rust and Martin, 1994). In line with our discussion in the Introduction, it may be noted that the result by Rust and Martin (1994) must be restricted to the end sections of filaments; it does not necessarily hold for their shape as a whole (which is a reverse S for the long, erupting filament in the event under consideration).

The filament eruption begins with a brightening of the aforementioned winding thread. The brightening appears to propagate from the position of the thread under the centre of the East – West filament arm towards both sides (02:32:13 – 02:47:27 UT; Figures 12b – 12d), which is consistent with magnetic reconnection occurring below the filament. The rise of the filament then starts immediately. As the filament rises, it first releases some of its tension by connecting the end points in a more straight manner than before the eruption (02:47:27 – 02:56:12 UT; Figure 12e). This gives an apparent clockwise rotation of the East – West arm and an apparent simultaneous counterclockwise rotation of the North – South arm, neither of which primarily represents the transformation of twist into writhe that we discuss

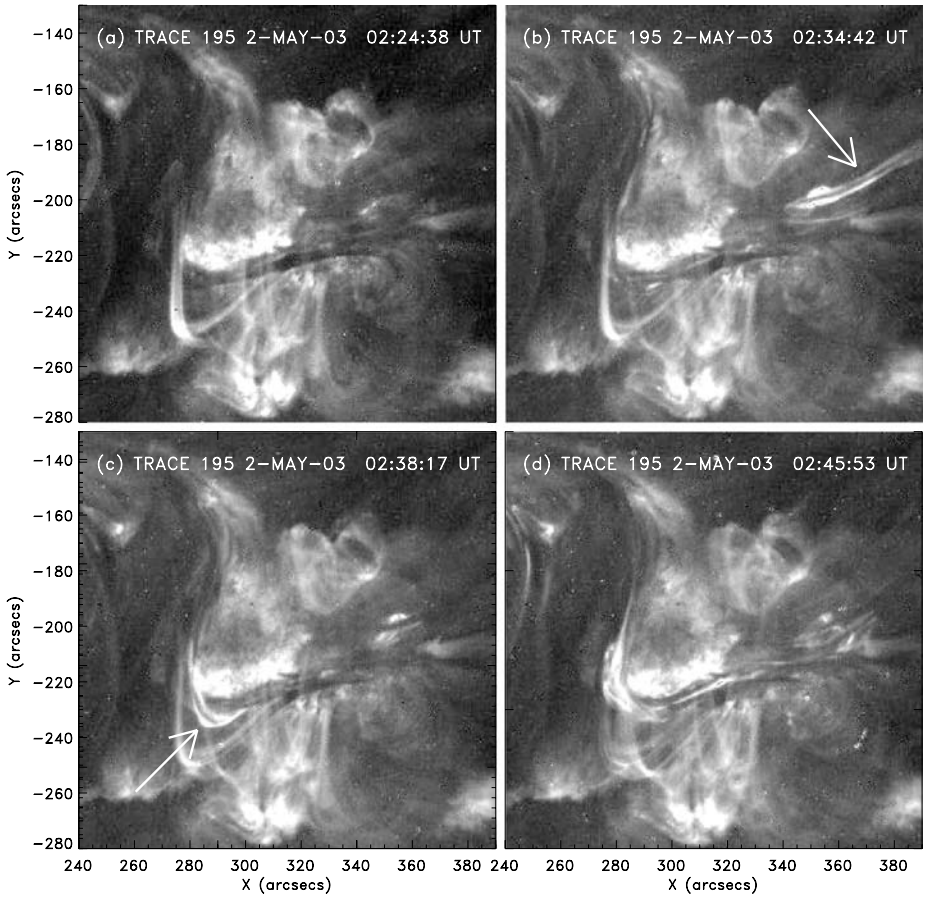

Figure 12 TRACE 195 Å waveband images of the filament eruption on 2 May 2003. The eruption begins with a brightening that propagates outwards from the centre of the East – West arm shown by arrows in (b) and (c). During the rise, the filament relaxes its shape (e) whilst simultaneously a clockwise rotation of the East – West arm occurs. This rotation is advanced in (f) and (g). Sigmoid formation and expansion occurs in (e) – (h).

in this paper. Overlapping in time with the straightening, the middle section of the erupting filament starts to rotate as a whole in the clockwise direction (02:55:27 – 02:58:00 UT; Figures 12e – 12g), which is consistent with the transformation of right-handed twist into writhe. In the process, the reverse-S shape becomes more pronounced again. Only very faint emitting threads outline the remnants of the filament in this phase. The appearance is considerably complicated by the highly irregular forms that the mixed threads in the south-western part of the erupting filament (between the rotating central part and the footpoint at the western end of the filament) develop. This part of the erupting structure contains the major fraction of the brightened ascending filament material. These brightenings are overlaid on brightenings at the bottom of the corona, which extend along the original East – West filament arm. The resulting brightening patterns are highly complex and variable. Nevertheless, the central section of the brightened erupting filament indicates the development of

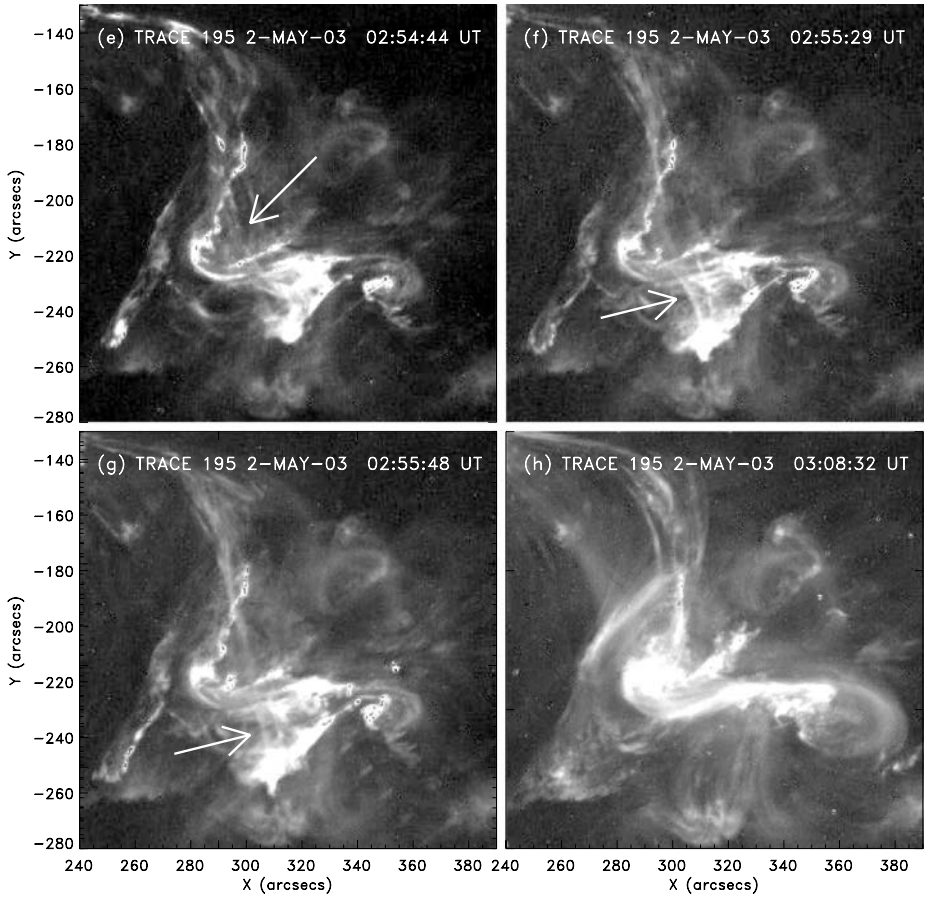

Figure 12 (Continued).

a reverse-S shape throughout its rotation phase (Figures 12e – 12g). The TRACE "Picture of the Day" Web site (http://trace.lmsal.com/POD/TRACEpod.html) contains a movie of this event.

The brightenings along the original East – West filament arm show an overall sigmoidal arrangement from about 02:54 UT onwards, and by 03:07:30 UT a bright, S-shaped sigmoid has formed (Figures 12e – 12h). Its eastern half nearly coincides with the eastern half of the original East – West filament arm. Its western half rapidly expands beyond the western half of the arm during 02:56:31 – 03:08:04 UT, but it retains its shape in the expansion. The sigmoid does not exhibit any signature of rotation.

Overall, this event shows a rising filament of right-handed helicity whose middle section rotates clockwise during the ascent, while near the end of the rotation a forward S-shaped sigmoid forms that neither appears to rise nor appears to rotate (*i.e.*, the sigmoid apparently formed under the erupting field and close to the original East – West filament arm). From the TRACE movie and from the absence of a CME in SOHO/LASCO observations we conclude that, very likely, the erupting filament stayed confined to the Sun.

5.7. Discussion of Incomplete S-Shape Observation and the Filament Eruption on 27 May 2002

We note that none of the events presented so far clearly show the development of a *complete* S shape of the filament during eruption. Instead, it is implied by the observed rotation of the filament's middle section, if we assume that the footpoints of the associated unstable flux rope are line-tied to the photosphere. There are several reasons why observing the expected S shape is difficult. First, to see the S shape clearly, one has to observe the filament almost perfectly in vertical projection on the solar disc. A different viewing angle would not reveal it directly. Second, the apex rotation typically requires a significant height range to fully develop. When observed in the EUV, the rising filament has then often expanded so strongly in the lateral direction that it becomes difficult to trace its axis (for example, the 15 June 2001 event). Also, the filament material may have drained down the legs so that the axis near its apex cannot be traced at all. When observed in Hα, the observation is even more difficult to make, since the Doppler-shifted rising central part soon escapes the narrow wavelength range. Third, as discussed in Section 1, filaments are often curved prior to eruption, especially in active regions as they spiral into the periphery of the main sunspots. Therefore, for the erupting filament to develop the opposite-S shape clearly, its apex has to undergo a significant rotation. Although rotations of the order of 90° or more are possible if the eruption is driven by the helical kink instability (*e.g.*, Török and Kliem, 2005; Fan and Gibson, 2003), much smaller rotations occur if the eruption is driven by other processes, for example by the torus instability (Kliem and Török, 2006). In such cases, one can observe the direction of apex rotation, but a clear S shape is not produced.

Here we present a case of a filament eruption and a numerical simulation of the event from which we can infer the occurrence of a complete S shape. Figure 13 shows TRACE images of the failed filament eruption in NOAA active region 9957 on 27 May 2002. This filament kept a clearly traceable form up to the point of maximum elevation shown in the final panel. Török and Kliem (2005) reproduced the morphology and rise profile of the filament in a numerical simulation of a kink-unstable flux rope, in very good agreement with the observations. A flux rope with positive chirality had to be used to account for the observed clockwise filament rotation, confirming the conclusion of Rust and LaBonte (2005) and Alexander, Liu, and Gilbert (2006) obtained from the TRACE images. A dominantly positive chirality of the active region is also indicated by calculating the $\alpha_{\rm best}$ value of magnetograms (taken at Marshall Space Flight Center on 22 and 23 May when the active region was near central meridian); the values consistently turned out to agree with the maximum permitted α for the given magnetogram size. It is also worth noting that MDI data show cancellation of the magnetic polarities occurring along the polarity inversion line during the active region's disc passage.

In contrast to TRACE, the simulation is not limited to a fixed viewing angle and can therefore help us study how the filament eruption would have looked in projection onto the photosphere. Figure 14 shows the filament during its rise phase at 18:05 UT (before shredding of the flux rope sets in), together with two different views of a corresponding snapshot from the simulation. At this stage of the simulation, the (initially straight) flux rope has already rotated clockwise by almost 90°, yielding a clear reverse-S shape, whereas the field lines below the flux rope exhibit a forward-S shape. From the very good agreement of the simulation with the observation, we conclude that the filament would have shown a clear reverse-S shape if it could have been observed from above.

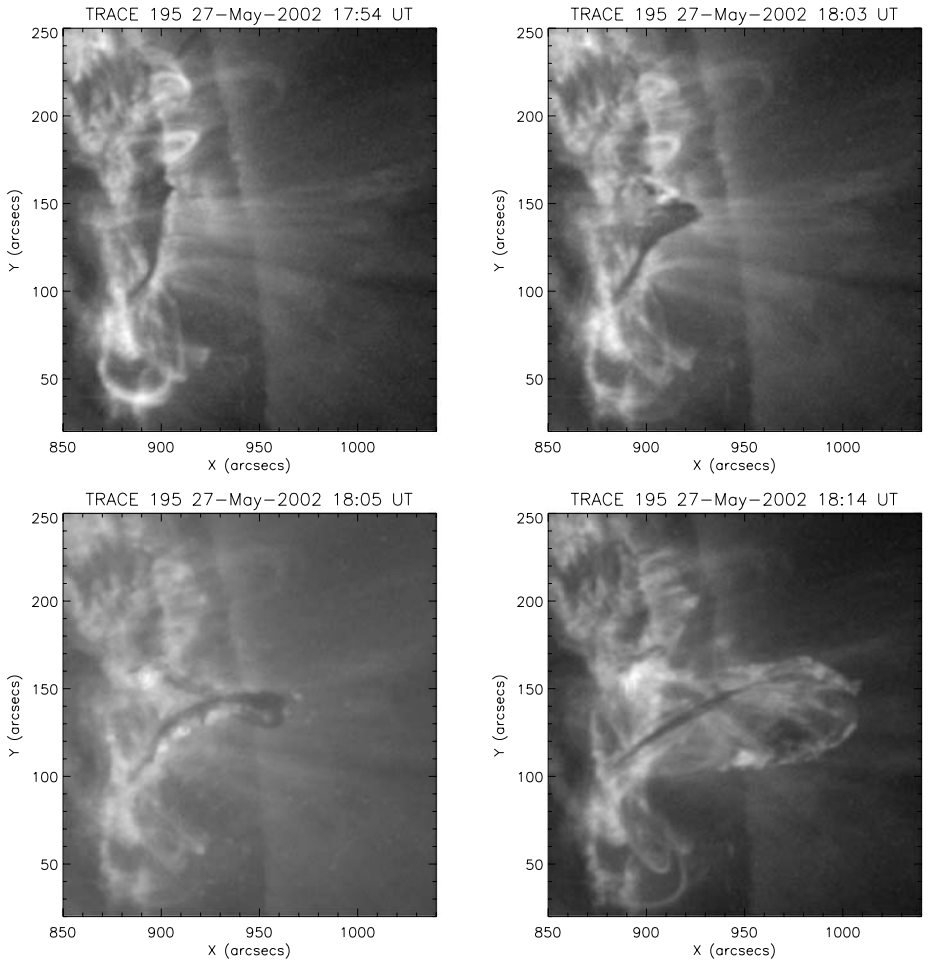

Figure 13 TRACE 195 Å waveband images of the filament eruption on 27 May 2002 in active region 9957. The axis of the filament is observed to rotate clockwise on eruption.

6. Discussion and Conclusions

We present a multiwavelength study of a sample of active regions which produce filaments that rotate upon eruption, determine the chirality of the erupting field, and compare the results to models of sigmoid formation. The relationship between chirality of the field, orientation of the transient sigmoid, and writhing (apex rotation) of the associated erupting filament obtained from the observations are summarised in Table 2. The following is found:

1. Sigmoids formed in association with the eruption of fields with positive (negative) helicity exhibit a forward (reverse) S shape, consistent with the results of Pevtsov, Canfield, and McClymont (1997).
2. The associated erupting (ascending) filaments rotate clockwise (counterclockwise), so that the resulting S shape of the flux rope implied by the direction of filament rotation is opposite to that of the sigmoid (where SXR or EUV data were available).

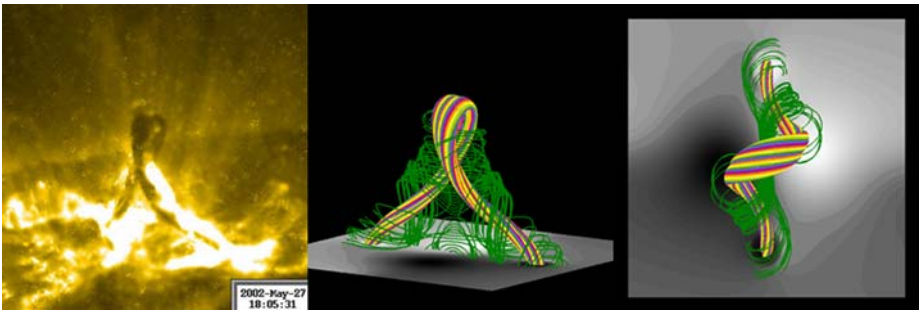

Figure 14 Comparison of the filament eruption on 27 May 2002 with the numerical simulation of Török and Kliem (2005). The coloured field lines outline the core of the kink-unstable flux rope. Additional field lines below the flux rope core are shown in green. The "magnetogram" of the normal component of the magnetic field in the bottom plane of the simulation box is included. The plot on the right shows a view from above at the same time as the plot in the middle.

Table 2 Summary table showing the results from each active region. "S" indicates a forward-S sigmoid and "Z" indicates a reverse-S sigmoid. The observations used for determining the helicity sign of the erupting field are listed in column 2 and the direction of rotation of the filament is shown in the last column. CW indicates a clockwise rotation and CCW indicates a counterclockwise rotation.

Date	Helicity indicator	Helicity sign	Sigmoid shape	Filament rot.
07 Apr 97	"sinistral" filament; flare ribbons; magnetic tongues	> 0	S	CW
12 May 97	"dextral" filament; flare ribbons	< 0	Z	CCW
06 Jun 00	filament threads; "dextral" filament; $\alpha(x, y)$	< 0	Z	CCW
19 Jul 00	filament threads; flare ribbons; α_{best}	< 0	Z	CCW
15 Jun 01	"dextral" filament; flare ribbons	< 0	Z	CCW
02 May 03	filament threads; "sinistral" filament	> 0	S	CW

The fact that the apex of the selected filaments rotates supports our assumption that they are contained in a magnetic flux rope, at least in the eruption stage; the rotation is regarded as a writhing of the flux rope. The direction of rotation, controlled by helicity conservation, provides independent support of our chirality determinations. In this work the chirality of the erupting field is determined directly; that is, we do not require the assumption that the dominant chirality of the active region (determined by the "alpha-best" method as in Pevtsov, Canfield, and McClymont, 1997, or by using magnetic tongues of newly emerging flux) also applies to the erupting field and sigmoid source.

The results are in full agreement with the predictions or implications of the Titov and Démoulin model, which associates sigmoids with enhanced dissipation in a layer of steepened current density, which forms under a dynamic flux rope and is threaded by sigmoidal field lines.

The results are also in line with the sigmoid – chirality relationship implied in the tether-cutting model, which associates the sigmoid with reconnection taking place in the core of a sheared arcade (where the sheared field can also support filament material). This reconnection also simultaneously forms a flux rope above the sigmoid and can lead to an ejection of the flux rope. However, even though this model implies the correct sigmoid – chirality association, the initial magnetic topology being that of a sheared arcade is not strongly supported by our observations. Indeed, many previous studies have suggested that the pre-eruption topology of a filament is that of a flux rope and not a sheared arcade (Section 1).

The suggestion of sigmoid formation *within* erupting flux ropes (Rust and Kumar, 1996) is not supported by our results. The relationship between the S shape of a rising unstable flux rope and its chirality is opposite to that seen in the observations of sigmoids. Furthermore, the only rotating motion observed in all the events is exhibited by the erupting filament and not by the sigmoid as is implied by this model.

The model would be consistent with the observed sigmoid – chirality relationship if the filament eruption would consist of a downward kinking of the original flux rope apex. Although such a scenario is conceivable for confined events (Kliem, Titov, and Török, 2004), in general there is little room for downward kinking, because the filaments run very low above the solar surface, especially in active regions. Indeed, the imaging data of our event sample indicate upward motion of all erupting filaments, although several of them stayed confined to the Sun (6 June 2000, 19 July 2000, 27 May 2002, and, very likely, also 2 May 2003).

Likewise, the reverse-shear model for sigmoids by Kusano (2005), which also implies an identical orientation for the sigmoid and the kinked flux rope, is not supported by our findings. However, the present analysis does not rule this model out because most (and possibly all) of the active regions in our sample do not contain left- and right-handed chiralities in comparable fractions, as required by the model, but are dominated by field of one chirality. Whether or not the model is often realised in active regions with mixed chirality, and can account for the $\approx$10% of cases of sigmoid orientation not conforming to the dominant chirality of the active region (Pevtsov, Canfield, and McClymont, 1997), can be assessed only through studies of sigmoids formed in mixed-chirality active regions.

Acknowledgements We are grateful to the Global High Resolution Hα Network, operated by the Big Bear Solar Observatory, New Jersey Institute of Technology, for the provision of data, to Mitzi Adams for providing us with the Marshall Space Flight Center Vector Magnetograph data of AR 9957, and to Tom Metcalf for providing us with the Mees Observatory vector magnetogram of AR 9077. We thank the anonymous referee for a very constructive report and Pascal Démoulin and Mitch Berger for very helpful comments on the manuscript. L.v.D.G. acknowledges the Hungarian government grant OTKA 048961. The work of B.K. was supported by the DFG and by NSF grant ATM 0518218 to the University of New Hampshire.

References

Alexander, D., Liu, R., Gilbert, H.R.: 2006, *Astrophys. J.* **653**, 719.
Amari, T., Luciani, J.F., Aly, J.J., Tagger, M.: 1996, *Astrophys. J.* **466**, L39.
Amari, T., Luciani, J.F., Mikic, Z., Linker, J.: 1999, *Astrophys. J.* **518**, L57.
Attrill, G.D.R., Nakwacki, M.S., Harra, L.K., van Driel-Gesztelyi, L., Mandrini, C.H., Dasso, S., Wang, J.: 2006, *Solar Phys.* **238**, 117.
Aulanier, G., Démoulin, P.: 1998, *Astron. Astrophys.* **329**, 1125.

Aulanier, G., Démoulin, P., Grappin, R.: 2005, *Astron. Astrophys.* **430**, 1067.
Aulanier, G., Srivastava, N., Martin, S.F.: 2000, *Astrophys. J.* **543**, 447.
Berger, M.A.: 1985, *Astrophys. J. Suppl.* **59**, 433.
Berger, M.A.: 2000a, *Plasma Phys. Control. Fusion* **41**, 167.
Berger, M.A.: 2000b, *Encyclopedia of Astronomy and Astrophysics*, Institute of Physics, Bristol, 2403.
Berger, M.A., Field, G.B.: 1984, *J. Fluid Mech.* **147**, 133.
Berger, M.A., Prior, C.: 2006, *J. Phys. A: Math. Gen.* **39**, 8321.
Brown, D.S., Nightingale, R.W., Alexander, D., Schrijver, C.J., Metcalf, T.R., Shine, R.A., Title, A.M., Wolfson, C.J.: 2003, *Solar Phys.* **216**, 79.
Burnette, A.B., Canfield, R.C., Pevtsov, A.A.: 2004, *Astrophys. J.* **606**, 565.
Canfield, R.C., Hudson, H.S., McKenzie, D.E.: 1999, *Geophys. Res. Lett.* **26**, 627.
Chae, J.: 2000, *Astrophys. J.* **540**, L115.
Démoulin, P., Priest, E.R., Lonie, D.P.: 1996, *J. Geophys. Res.* **101**, 7631.
DeVore, C.R., Antiochos, S.K.: 2000, *Astrophys. J.* **539**, 954.
Fan, Y., Gibson, S.E.: 2003, *Astrophys. J.* **589**, L105.
Fan, Y., Gibson, S.E.: 2004, *Astrophys. J.* **609**, 1123.
Gibson, S.E., Fletcher, L., Del Zanna, G., Pike, C.D., Mason, H.E., Mandrini, C.H., Démoulin, P., Gilbert, H., Burkepile, J., *et al.*: 2002, *Astrophys. J.* **574**, 1021.
Gibson, S.E., Fan, Y., Mandrini, C., Fisher, G., Demoulin, P.: 2004, *Astrophys. J.* **617**, 600.
Gibson, S.E., Fan, Y., Török, T., Kliem, B.: 2006, *Space Sci. Rev.* **124**, 131.
Hagino, M., Sakurai, T.: 2004, *Publ. Astron. Soc. Japan* **56**, 831.
Hale, G.E.: 1925, *Publ. Astron. Soc. Pac.* **37**, 268.
Handy, B.N., Acton, L.W., Kankelborg, C.C., Wolfson, C.J., Akin, D.J., Bruner, M.E., Caravalho, R., Catura, R.C., Chevalier, R., *et al.*: 1999, *Solar Phys.* **187**, 229.
Ji, H., Wang, H., Schmahl, E.J., Moon, Y.-J., Jiang, Y.: 2003, *Astrophys. J.* **595**, L135.
Kliem, B., Török, T.: 2006, *Phys. Rev. Lett.* **96**, 255002.
Kliem, B., Titov, V.S., Török, T.: 2004, *Astron. Astrophys.* **413**, L23.
Kusano, K.: 2005, *Astrophys. J.* **631**, 1260.
Kusano, K., Maeshiro, T., Yokoyama, T., Sakurai, T.: 2004, *Astrophys. J.* **610**, 537.
Lionello, R., Mikić, Z., Linker, J.A., Amari, T.: 2002, *Astrophys. J.* **581**, 718.
López Fuentes, M.C., Démoulin, P., Mandrini, C.H., van Driel-Gesztelyi, L.: 2000, *Astrophys. J.* **544**, 540.
Low, B.C.: 1996, *Solar Phys.* **167**, 217.
Low, B.C., Berger, M.A.: 2003, *Astrophys. J.* **589**, 644.
Manoharan, P.K., van Driel-Gesztelyi, L., Pick, M., Démoulin, P.: 1996, *Astrophys. J.* **468**, L73.
Martens, P.C., Zwaan, C.: 2001, *Astrophys. J.* **558**, 872.
Martin, S.F.: 1998, *Solar Phys.* **182**, 107.
Martin, S.F., Billimoria, R., Tracadas, P.W.: 1994, In: Rutten R.J., Schrijver C.J. (eds.) *Solar Surface Magnetism*, *NATO ASI Ser. C* **433**, Kluwer, Dordrecht, 303.
Moore, R.L., LaBonte, B.J.: 1980, In: Dryer M., Tandberg-Hanssen E. (eds.) *Solar and Interplanetary Dynamics*, *IAU Symp.* **91**, Reidel, Boston, 207.
Moore, R.L., Roumeliotis, G.: 1992, In: Svestka, Z., Jackson, B.V., Machado, M.E. (eds.) *Eruptive Solar Flares*, Springer, Berlin, 69.
Moore, R.L., Sterling, A.C., Hudson, H.S., Lemen, J.R.: 2001, *Astrophys. J.* **552**, 833.
Nakagawa, Y., Raadu, M.A., Billings, D.E., McNamara, D.: 1971, *Solar Phys.* **19**, 72.
Pevtsov, A.A.: 2002a, In: Martens P.C.H., Cauffman D. (eds.) *Multi-Wavelength Observations of Coronal Structure and Dynamics*, *COSPAR Colloq. Ser.* **13**, Elsevier, Amsterdam, 125.
Pevtsov, A.A.: 2002b, *Solar Phys.* **207**, 111.
Pevtsov, A.A., Canfield, R.C., Metcalf, T.R.: 1995, *Astrophys. J.* **440**, L109.
Pevtsov, A.A., Canfield, R.C., McClymont, A.M.: 1997, *Astrophys. J.* **481**, 973.
Priest, E.R., Hood, A.W., Anzer, U.: 1989, *Astrophys. J.* **344**, 1010.
Priest, E.R., van Ballegooijen, A.A., Mackay, D.H.: 1996, *Astrophys. J.* **460**, 530.
Romano, P., Contarino, L., Zuccarello, F.: 2003, *Solar Phys.* **214**, 313.
Romano, P., Contarino, L., Zuccarello, F.: 2005, *Astron. Astrophys.* **433**, 683.
Rust, D.M.: 2003, *Adv. Space Res.* **32**, 1895.
Rust, D.M., Kumar, A.: 1994, *Solar Phys.* **155**, 69.
Rust, D.M., Kumar, A.: 1996, *Astrophys. J.* **464**, L199.
Rust, D.M., LaBonte, B.J.: 2005, *Astrophys. J.* **622**, L69.
Rust, D.M., Martin, S.: 1994, In: Balasubramaniam, K.S., Simon, G.W. (eds.) *Solar Active Region Evolution: Comparing Models with Observations*, *ASP Conf. Ser.* **68**, Astron. Soc. Pac., San Francisco, 337.
Ruzmaikin, A., Martin, S., Hu, Q.: 2003, *J. Geophys. Res.* **108**, 13.

Scherrer, P.H., Bogart, R.S., Bush, R.I., Hoeksema, J.T., Kosovichev, A.G., Schou, J., Rosenburg, W., Springer, L., Tarbell, T.D., *et al.*: 2005, *Solar Phys.* **162**, 129.
Seehafer, N.: 1990, *Solar Phys.* **125**, 219.
Shibata, K.: 1998, *Astrophys. Space Sci.* **264**, 129.
Song, L., Zhang, J., Yang, Z., Wang, W.: 2002, *Solar Phys.* **211**, 315.
Titov, V.S., Démoulin, P.: 1999, *Astron. Astrophys.* **351**, 707.
Titov, V.S., Démoulin, P., Hornig, G.: 1999, In: Wilson, A. (ed.) *Magnetic Fields and Solar Processes*, *SP-***448**, ESA, Noordwijk, 715.
Titov, V.S., Galsgaard, K., Neukirch, T.: 2003, *Astrophys. J.* **582**, 1172.
Török, T., Kliem, B.: 2003, *Astron. Astrophys.* **406**, 1043.
Török, T., Kliem, B.: 2005, *Astrophys. J.* **630**, L97.
Török, T., Kliem, B.: 2007, *Astron. Nachr.* **328**, 743.
Török, T., Kliem, B., Titov, V.S.: 2004, *Astron. Astrophys.* **413**, L27.
Tsuneta, S., Acton, L., Bruner, M., Lemen, J., Brown, W., Caravalho, R., Catura, R., Freeland, S., Jurcevich, B., *et al.*: 1991, *Solar Phys.* **136**, 37.
Webb, D.F., Lepping, R.P., Burlaga, L.F., DeForest, C.E., Larson, D.E., Martin, S.F., Plunkett, S.P., Rust, D.M.: 2000, *J. Geophys. Res.* **105**, 27251.
Williams, D.R., Török, T., Démoulin, P., van Driel-Gesztelyi, L., Kliem, B.: 2005, *Astrophys. J.* **628**, L163.
Woltjer, L.: 1958, *Proc. Nat. Acad. Sci. USA* **44**, 480.
Zhang, H.: 2002, *Mon. Not. Roy. Astron. Soc.* **332**, 500.
Zhang, H.: 2006, *Chin. J. Astron. Astrophys.* **6**, 96.